ACS Photonics

Letter

Cite This: ACS Photonics 2018, 5, 3466−3471

pubs.acs.org/journal/apchd5

Radiative Enhancement of Single Quantum Emitters in WSe_2 Monolayers Using Site-Controlled Metallic Nanopillars

Tao Cai,[†,‡] Je-Hyung Kim,[†,§] Zhili Yang,[†] Subhojit Dutta,[†] Shahriar Aghaeimeibodi,[†] and Edo Waks*[,†,‡]

[†]Department of Electrical and Computer Engineering and Institute for Research in Electronics and Applied Physics, University of Maryland, College Park, Maryland 20742, United States

[‡]Joint Quantum Institute, University of Maryland and the National Institute of Standards and Technology, College Park, Maryland 20742, United States

[§]Department of Physics, Ulsan National Institute of Science and Technology (UNIST), Ulsan 44919, Republic of Korea

Supporting Information

ABSTRACT: Plasmonic nanostructures provide an efficient way to control and enhance the radiative properties of quantum emitters. Coupling these structures to single defects in two-dimensional materials provides a particularly promising material platform to study emitter−plasmon interactions because these emitters are not embedded in a surrounding dielectric. They can therefore approach a near-field plasmonic mode to nanoscale distances, potentially enabling strong light−matter interactions. However, this coupling requires precise alignment of the emitters to the plasmonic mode of the structures, which is particularly difficult to achieve in a site-controlled structure. We present a technique to generate quantum emitters in two-dimensional tungsten diselenide coupled to site-controlled plasmonic nanopillars. The plasmonic nanopillar induces strains in the two-dimensional material which generate quantum emitters near the high-field region of the plasmonic mode. The electric field of the nanopillar mode is nearly parallel to the two-dimensional material and is therefore in the correct orientation to couple to the emitters. We demonstrate both an enhanced spontaneous emission rate and increased brightness of emitters coupled to the nanopillars. This approach may enable bright site-controlled nonclassical light sources for applications in quantum communication and optical quantum computing.

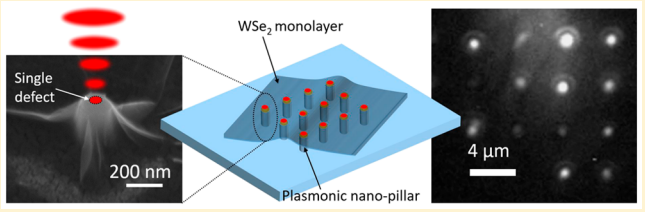

KEYWORDS: *quantum emitters, single-defect emitters, plasmonic nanopillars, two-dimensional semiconductors, transition-metal dichalcogenide, WSe_2*

Quantum emitters play an important role in many quantum optical applications, such as secured quantum communication,[1,2] quantum computation,[3,4] and quantum metrology.[5,6] Single-defect emitters in atomically thin materials[7−16] constitute a new class of nonclassical light sources that provides a two-dimensional platform to realize these quantum optical applications. Because they are two-dimensional in nature, these emitters do not suffer from dielectric screening effects and losses due to total internal reflection that hinder other solid-state emitters that are embedded in a material with a high refractive index. Moreover, they can be generated at desired locations by strain engineering,[17−23] which offers a simple and scalable approach to couple them to photonic devices.

Plasmonic nanostructures constitute an important class of photonic devices for coupling to quantum emitters.[24] These nanostructures concentrate light to subwavelength dimensions,[25,26] resulting in strong light−matter interactions that can enhance the brightness and emission rate of quantum emitters[27,28] and achieve strong optical nonlinearities.[29] Furthermore, emitter−plasmon structures offer the possibility to create optical devices that are significantly smaller than the wavelength of light[25,26] and operate at extremely high bandwidths.[30,31] Two-dimensional emitters are promising to couple to plasmonic nanostructures because they are not embedded in a dielectric material. They can therefore approach the plasmonic mode of a nanostructure to nanometer distances without being obstructed by the surrounding substrate, but achieving this coupling is challenging because of the stringent alignment requirement between the emitter and plasmonic mode which is in the nanometer size scale.[25,26] Such an accurate alignment in a site-localized device is particularly challenging because it requires accurate and simultaneous spatial control of the plasmonic mode and emitter. Atomic force microscope tips can position plasmonic nanostructures close to a quantum emitter,[32] but this approach requires a complicated experimental apparatus and is not easily scalable to multiple devices. Other methods employ an emitter positioned on a dense array of plasmonic nanostructures[33] or

Received: May 3, 2018
Published: August 24, 2018

DOI: 10.1021/acsphotonics.8b00580
ACS Photonics 2018, 5, 3466−3471

generated at a roughened metallic surface[34] in order to ensure the emitter is coupled to at least one localized plasmonic mode, but these approaches are still random and require a large device area. Metal nanowires can also efficiently couple to two-dimensional emitters[22] but exhibit delocalized propagating surface plasmons with large mode volumes, as opposed to localized plasmons that support tight field confinement and strong light−matter coupling. The ability to create site-localized plasmon-emitter structures with high efficiency remains a difficult problem.

Here we present a technique to generate quantum emitters in two-dimensional semiconductors coupled to site-controlled plasmonic nanopillars. A lithographically defined plasmonic nanopillar induces strains in a tungsten diselenide (WSe_2) monolayer, leading to the generation of single-defect emitters self-aligned to the plasmonic mode. By taking statistics over many devices, we demonstrate an increased brightness and enhanced spontaneous emission rate in the emitters coupled to plasmonic nanopillars. These results confirm that plasmonic nanopillars induce strong light−matter coupling. Our results could find applications in nanoscale ultrafast single-photon sources with controlled positions[27,28] as well as in compact nonlinear optical devices operating near the single-photon level.[29,35−38]

Figure 1a shows a schematic of the plasmonic nanopillar device design, which is composed of a silicon nanopillar with a

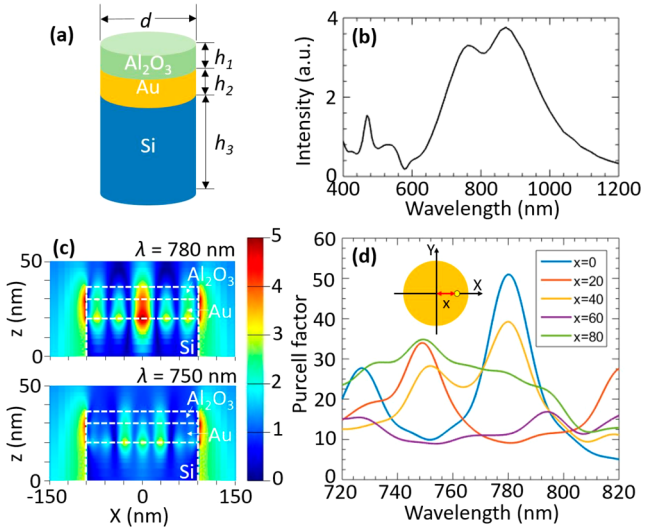

Figure 1. (a) Schematic layout of a single plasmonic nanopillar; d = 180 nm, h_1 = 6 nm, h_2 = 10 nm, and h_3 = 280 nm. (b) Numerically calculated scattering spectrum of a single plasmonic nanopillar. (c) Simulated distribution of electric field $|E_x|$ at the top of a plasmonic nanopillar at 780 nm (top panel) and 750 nm (bottom panel). (d) Calculated Purcell factors of an emitter by varying its wavelength and relative position to a nanopillar. Each curve corresponds to an emitter with a particular distance from the center of the nanopillar. The dipole orientation of the emitter is set to be parallel to the x-axis of the coordinate as shown in the inset.

10 nm thick gold layer and a 6 nm thick aluminum oxide (Al_2O_3) layer on top. We choose a gold film because it suffers less from oxidation compared to other metals such as silver, which is essential in bringing the emitters close to the high-field region of the plasmonic structure. We introduce the Al_2O_3 thin film as a buffer layer to prevent quenching of the emission of WSe_2 monolayer,[39] as well as to passivate it to reduce spectral wandering and blinking.[15] The nanopillar has a diameter of 180 nm and an overall height of about 300 nm. Figure 1b shows the numerically calculated scattering spectrum of the plasmonic structure determined using a finite-difference time-domain (FDTD) method (FDTD solutions, Lumerical), which suggests a broadband enhancement to the emitters (a typical emission range of these single defects is from 720 to 820 nm). The electric field distribution of the nanopillar has a dependence on its wavelength. Figure 1c shows the simulated profiles of electric field along the x-axis at 780 and 750 nm, representing two distinct field distributions. The wavelength dependence of the field profile leads to varied enhancements to the emitters with different wavelengths and relative positions to the nanopillar. To further confirm this, we also explore the Purcell effect of an emitter sitting on top of the nanopillar by varying its wavelength and position. To calculate the Purcell factor, we compare decay rates of a dipole with and without the plasmonic structure. Figure 1d concludes the calculated Purcell factors, which exhibit strong dependence on both the wavelength and the position of an emitter (see the Supporting Information for an example calculation of the position dependence, Figure S1). We notice that the scattering spectrum in Figure 1b exhibits a broader line width than that of the Purcell factors shown in Figure 1d. This is because each curve in Figure 1d corresponds to the enhancement at a particular position relative to the nanopillar, while the scattering spectrum shows an overall effect averaged over positions.

Figure 2a illustrates the device fabrication procedure. To prepare the sample, we first spin coat negative resist (ma-N

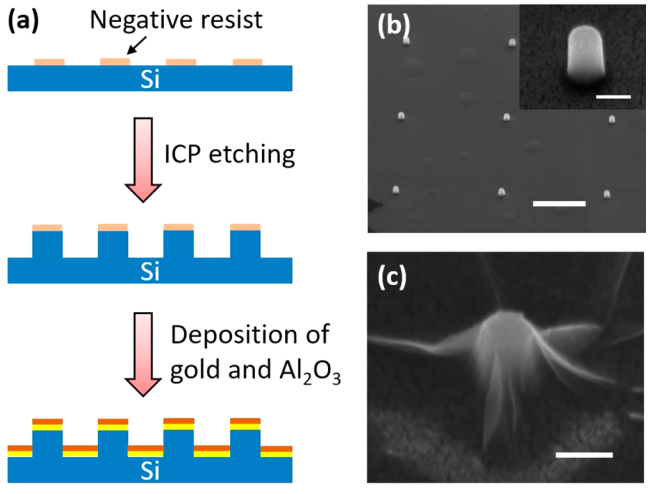

Figure 2. (a) Flowchart of the fabrication procedure of the plasmonic nanopillars. (b) Scanning electron micrograph showing a part of the array of plasmonic nanopillars. Scale bar: 2 μm. Inset: close-up of a single plasmonic nanopillar. Scale bar: 200 nm. (c) Scanning electron micrograph showing a single plasmonic nanopillar covered by a WSe_2 monolayer. Scale bar: 200 nm.

2401, MicroChem) on the silicon substrate and pattern the resist using e-beam lithography. We then transfer the pattern from the resist to the silicon substrate using inductively coupled plasma (ICP) dry etching. We deposit the gold layer using thermal evaporation, followed by atomic layer deposition to deposit the Al_2O_3 buffer. The final device consists of a 30 × 30 array of nanopillars arranged in a square matrix, separated by 4 μm. Figure 2b shows a scanning electron micrograph of a

DOI: 10.1021/acsphotonics.8b00580
ACS Photonics 2018, 5, 3466−3471

small region of the fabricated device, with the inset showing a close-up of a single nanopillar. Following the pillar fabrication, we transfer WSe_2 monolayers synthesized by chemical vapor deposition on a sapphire substrate,[40] onto the pillars using a polydimethylsiloxane (PDMS) substrate as an intermediate transfer medium.[41] Figure 2c shows a scanning electron micrograph of one plasmonic nanopillar covered by a flake of WSe_2.

To characterize the sample optically, we first cool it to a base temperature of 3 K using a closed-cycle refrigerator (attoDRY, Attocube Inc.). We perform all photoluminescence measurements using a confocal microscope. An objective lens with a numerical aperture of 0.8 serves to both focus the excitation laser and collect the emitted fluorescence signal. By adjusting the collimation of the input laser, we control the size of the focus to attain either a small diffraction-limited spot that excites a single nanopillar or a large spot that excites an area covering multiple pillars for wide-field imaging using a CCD camera (Rolera-XR, Qimaging Inc.). A 715 nm long-pass optical filter (Semrock Inc.) rejects the pump wavelength to isolate the fluorescence signal. A single-mode fiber spatially filters the signal to the diffraction limit and sends it to a grating spectrometer (SP2750, Princeton Instruments) for high-resolution spectral measurements. The output of the spectrometer connects to a Hanbury Brown and Twiss intensity interferometer that performs two-photon correlation and lifetime measurements.

Figure 3a shows a photoluminescence intensity map of the sample. We excite the sample using a continuous-wave laser emitting at 532 nm, with a large excitation spot that covers multiple nanopillars. Each nanopillar introduces a deformation in the atomically thin WSe_2 that covers it, leading to the generation of strain-induced single defects in close proximity to the plasmonic mode,[17−23] as evidenced by the bright emission from all nanopillars in the array. To confirm that the emission originates from single defects, we measure the photoluminescence spectrum from a single nanopillar using a tightly focused spot. Figure 3b shows the spectrum of a representative nanopillar that exhibits a sharp emission line. The full width at half-maximum (fwhm) of this emitter is about 0.55 nm. We notice that the emission peak is asymmetric, which we attribute to the phonon sideband.[42,43] The spectrum of the observed emitter is distinct from the photoluminescence coming from the bare WSe_2 monolayer area which exhibits a broadband emission (see Figure S2). Depending on the emitter, we can observe both singlet and doublet spectral emission lines (see Figure S3). Both line shapes are consistent with previously reported spectra from defects in WSe_2 monolayer.[8−12,44] Previous results attribute the origin of the doublet to be the mixing of the two neutral excitonic states due to the electron−hole spin-exchange interaction, while the origin of the singlet remains unclear. Because emitters are formed by a strain-driven process, the number of emitters in each nanopillar can vary. Figure 3b shows an example where we observe only a single peak corresponding to one emitter, while other pillars exhibit multiple peaks (see Figure S4).

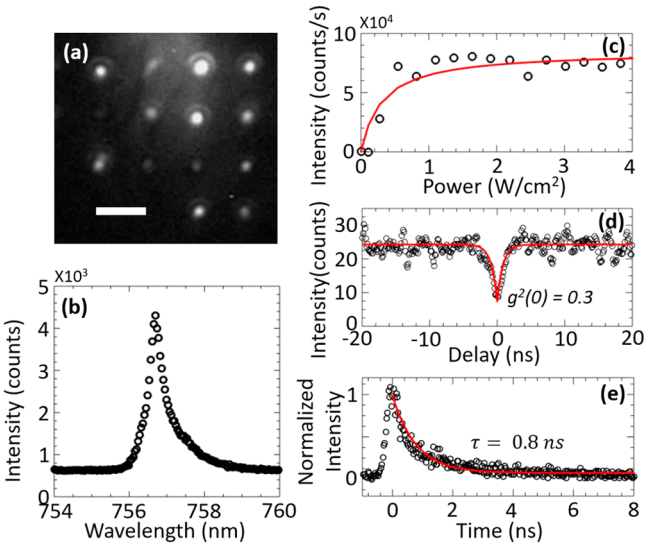

Figure 3. (a) Photoluminescence intensity map of arrays of plasmonic nanopillars covered by WSe_2 monolayer. Scale bar: 4 μm. (b) Photoluminescence spectrum of a representative emitter. (c) Emission intensity of the emitter in panel b as a function of the excitation power (black circles), fitted to a saturation function (solid red curve). (d) Second-order correlation measurement of the emitter in panel b (black circles) fitted to a double-exponential decay function (solid red curve). (e) Time-resolved photoluminescence of the emitter in panel b (black circles), fitted to a single-exponential decay function (solid red curve).

In Figure 3c we plot the emission intensity of the emitter shown in Figure 3b as a function of the excitation power, using a 532 nm continuous-wave excitation source. The intensity shows a saturation behavior that is consistent with emission from a localized single emitter. We fit the measured data to a saturation function of the form $I = I_{sat}P/(P_{sat} + P)$, where I and I_{sat} are the integrated intensity and the saturation intensity, respectively, and P and P_{sat} are excitation power and saturation power, respectively. In the fit, we treat I_{sat} and P_{sat} as fitting parameters and set a 90% confidence interval. From the fit we determine a saturation power of 0.31 ± 0.18 W/cm^2 (before the objective lens) and a saturation intensity of 8.50 ± 0.88 × 10^4 counts/s on the single-photon counting module. Because of the discretization of the excitation power we use, there are not many data points below saturation. Also, we note that the emitter exhibits a fluctuation in its intensity, leading to the shot noise in the measurement. However, the saturation behavior of the emitter is very clear. Also, a reasonable number of data points above saturation offers the accuracy of the fitting for the saturation intensity.

To further validate that the emission originates from a single defect and show that the defect acts as a quantum light source, we perform a second-order correlation measurement. Figure 3d shows the second-order correlation measurement under continuous-wave excitation of the emitter shown in Figure 3b. By fitting the measured data to a double-exponential decay function, we calculate a $g^2(0) = 0.3$, which drops below the threshold for photon antibunching of 0.5. This confirms that the emission originates from a single photon emitter.

From the exponential fitting to the curve in Figure 3d, we calculate a lifetime of 0.8 ns, which is shorter than the usual lifetimes (a few nanoseconds) of single defects in WSe_2 monolayer.[8−12,17−21] We perform a time-resolved photoluminescence measurement to further confirm the lifetime of the emitter. We excite the emitter using 710 nm laser pulses with a 2 ps pulsewidth, aligning to the exciton of the WSe_2 monolayer (see Figure S2), and directly measure the fluorescence decay. By fitting the measured lifetime in Figure 3e to an exponential decay, we calculate a lifetime of 0.8 ns, which matches the result derived from the second-order

DOI: 10.1021/acsphotonics.8b00580
ACS Photonics 2018, 5, 3466−3471

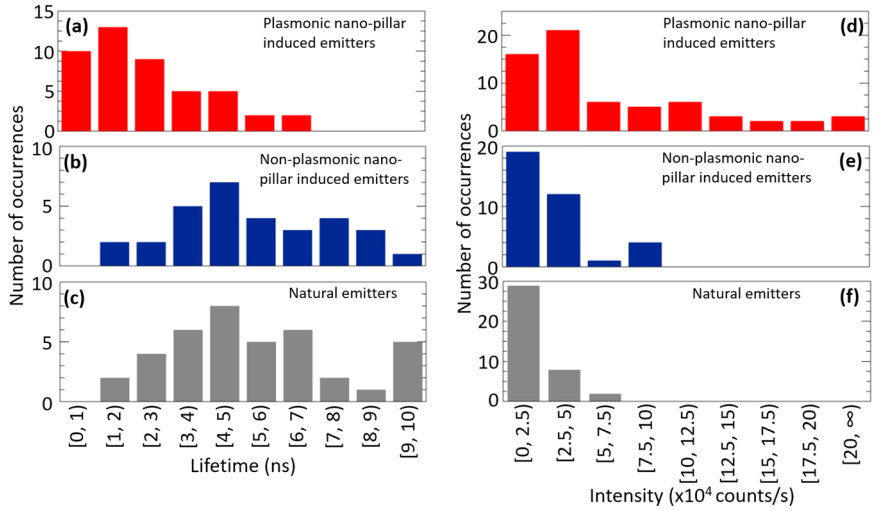

Figure 4. (a–c) Statistical comparison over lifetimes of single-defect emitters in WSe_2 monolayers. Distribution of lifetimes of (a) single defects induced by plasmonic nanopillars, (b) single defects induced by nonplasmonic nanopillars, and (c) natural single defects. (d–f) Statistical comparison over photoluminescence emission intensities of single-defect emitters in WSe_2 monolayers. Distribution of intensities of (d) single defects induced by plasmonic nanopillars, (e) single defects induced by nonplasmonic nanopillars, and (f) natural single defects.

correlation measurement. The reduced lifetime suggests an enhanced spontaneous emission rate (Purcell enhancement) due to coupling to the surface plasmon mode. However, even in a bare WSe_2 monolayer the single-defect emitters exhibit a large variation of lifetime and intensity (see Figure S5). Thus, it is difficult to conclude from the measurement of a single emitter whether a Purcell enhancement is present. To do so requires a statistical average of the lifetimes of many emitters. We perform these statistics using measurements from 46 different emitters (see the Supporting Information for examples of lifetime measurements, Figure S6). We compare the lifetimes of these emitters to a similar number of emitters in two control groups, one in the bare material with no nanopillars and the other with nanopillars that are not coated with gold and therefore exhibit no plasmonic mode confinement.

Figure 4a plots the distribution of lifetimes of the emitters in the plasmonic nanopillars, where we observe an average lifetime of 2.2 ± 1.5 ns, with a median lifetime of 1.8 ns. As a comparison, Figure 4b plots the distribution of lifetimes of 31 emitters in the nonplasmonic nanopillars (bare silicon nanopillars), exhibiting an average lifetime of 5.2 ± 2.1 ns with a median lifetime of 4.9 ns. Similarly, the 39 single-defect emitters naturally existing in the WSe_2 monolayer show an average lifetime of 5.3 ± 2.3 ns with a median lifetime of 5.0 ns, shown in Figure 4c. The observed average reduction in the lifetime of 2.4 indicates that the plasmonic nanopillars induce a Purcell effect.

We also statistically investigate the photoluminescence emission intensities of the single defects. To measure the emission intensities, we excite the emitters using a continuous-wave laser at 710 nm and measure the emission intensities at saturation using the spectrometer. Figure 4d–f plots the distribution of emission intensities of three groups of emitters. The emitters in close proximity to the plasmonic structures exhibit a median intensity of 4.4×10^4 counts/s. The emitters induced by nonplasmonic nanopillars and the natural emitters exhibit a median intensity of 2.3×10^4 and 0.6×10^4 counts/s, respectively. The observed increase in the emission intensities of the plasmonic nanopillar-induced emitters, combined with the increased decay rate, indicate an enhanced radiative decay rate of the emitters due to the coupling to the surface plasmon mode. This also excludes the possibility that quenching plays a major role in the modified lifetime, because otherwise we expect to see reduction both in the lifetime and brightness of the emitters.

Because of the large variation in the lifetime and intensity of the uncoupled emitters, observing a statistically significant correlation between the lifetime and intensity of the coupled emitters is extremely difficult (see Figure S7). Only when we average the lifetimes and intensities of all emitters do we obtain sufficient statistics to be able to claim a clear effect. When the emitters are subdivided into smaller groups by lifetime or intensity, the noise is large enough to wash out any significant trend. Also, we do not observe any clear correlation between the wavelength and radiative enhancement (see Figure S8). This is likely because the nanopillar resonance is broad compared to the inhomogeneous distribution of the emitters and also because the natural emitters exhibit large variation in lifetime so any underlying wavelength-dependent changes get washed out. Besides the variation in lifetime and intensity, we also observe a large fluctuation in the line width of these emitters (see Table S1). However, the emitters in the plasmonic nanopillars show a similar distribution in the line width as compared to the emitters in the other two control groups, which suggests that the line width is dominated by spectral wandering and the phonon sideband.

In conclusion, we presented a technique to generate quantum emitters in atomically thin semiconductors coupled to site-controlled plasmonic nanopillars. The lithographically defined plasmonic nanopillar induced strains in the WSe_2 monolayer, which formed single-defect emitters in close proximity to the plasmonic structure. Studies of multiple nanopillars revealed emitters with statistically shortened lifetimes and increased emission intensities as compared to those not coupled to plasmonic structures, indicating Purcell enhancement. The technique we presented here could be used to realize ultrafast nonclassical light sources[27,28] and nonlinear photonic devices.[29] The capability to control the position of the light source enables device integration with more complex

DOI: 10.1021/acsphotonics.8b00580
ACS Photonics 2018, 5, 3466–3471

quantum optical circuits and offers the possibility for scalable device fabrication. Although such a technique does not guarantee deterministic generation of emitters such that each nanopillar creates one single emitter, one can advance this technology toward deterministic arrays by spectrally filtering individual emitters from each post and incorporating spectral tuning techniques to tune them to the desired wavelength.[45] The technique is versatile and could be applied to construct coupled devices composed of various plasmonic nanostructures[24] and single defects in diverse atomically thin materials.[7−16]

■ ASSOCIATED CONTENT

Supporting Information

The Supporting Information is available free of charge on the ACS Publications website at DOI: 10.1021/acsphotonics.8b00580.

Position dependence of Purcell enhancement to an emitter; photoluminescence spectra of a bare WSe_2 monolayer area, representative nanopillar-induced single defects, and representative nanopillars exhibiting multiple peaks; lifetime versus photoluminescence intensity of naturally existing single defects in WSe_2 monolayers and of plasmonic nanopillar-induced emitters; time-resolved photoluminescence measurements of single-defect emitters in WSe_2 monolayers; lifetime versus wavelength of plasmonic nanopillar-induced emitters; line width of single-defect emitters in WSe_2 monolayers (PDF)

■ AUTHOR INFORMATION

Corresponding Author

*E-mail: edowaks@umd.edu.

ORCID

Tao Cai: 0000-0002-3264-6178

Je-Hyung Kim: 0000-0002-6894-9285

Notes

The authors declare no competing financial interest.

■ ACKNOWLEDGMENTS

The authors acknowledge support from the National Science Foundation (Award Number ECCS1508897), the Office of Naval Research ONR (Award Number N000141410612), the Air Force Office of Scientific Research (AFOSR) (Award Number 271470871D), and the Physics Frontier Center at the Joint Quantum Institute.

■ REFERENCES

(1) Duan, L.-M.; Lukin, M. D.; Cirac, J. I.; Zoller, P. Long-Distance Quantum Communication with Atomic Ensembles and Linear Optics. *Nature* **2001**, *414*, 413−418.

(2) Kimble, H. J. The Quantum Internet. *Nature* **2008**, *453*, 1023−1030.

(3) Loss, D.; DiVincenzo, D. P. Quantum Computation with Quantum Dots. *Phys. Rev. A: At., Mol., Opt. Phys.* **1998**, *57*, 120−126.

(4) Monroe, C. Quantum Information Processing with Atoms and Photons. *Nature* **2002**, *416*, 238−246.

(5) Giovannetti, V.; Lloyd, S.; Maccone, L. Quantum Metrology. *Phys. Rev. Lett.* **2006**, *96*, 010401.

(6) Giovannetti, V.; Lloyd, S.; Maccone, L. Advances in Quantum Metrology. *Nat. Photonics* **2011**, *5*, 222−229.

(7) Aharonovich, I.; Toth, M. Quantum Emitters in Two Dimensions. *Science* **2017**, *358*, 170−171.

(8) Srivastava, A.; Sidler, M.; Allain, A. V.; Lembke, D. S.; Kis, A.; Imamoğlu, A. Optically Active Quantum Dots in Monolayer WSe_2. *Nat. Nanotechnol.* **2015**, *10*, 491−496.

(9) Koperski, M.; Nogajewski, K.; Arora, A.; Cherkez, V.; Mallet, P.; Veuillen, J.-Y.; Marcus, J.; Kossacki, P.; Potemski, M. Single Photon Emitters in Exfoliated WSe_2 Structures. *Nat. Nanotechnol.* **2015**, *10*, 503−506.

(10) He, Y.-M.; Clark, G.; Schaibley, J. R.; He, Y.; Chen, M.-C.; Wei, Y.-J.; Ding, X.; Zhang, Q.; Yao, W.; Xu, X.; Lu, C.-Y.; Pan, J.-W. Single Quantum Emitters in Monolayer Semiconductors. *Nat. Nanotechnol.* **2015**, *10*, 497−502.

(11) Chakraborty, C.; Kinnischtzke, L.; Goodfellow, K. M.; Beams, R.; Vamivakas, A. N. Voltage-Controlled Quantum Light from an Atomically Thin Semiconductor. *Nat. Nanotechnol.* **2015**, *10*, 507−511.

(12) Tonndorf, P.; Schmidt, R.; Schneider, R.; Kern, J.; Buscema, M.; Steele, G. A.; Castellanos-Gomez, A.; van der Zant, H. S. J.; de Vasconcellos, S. M.; Bratschitsch, R. Single-Photon Emission from Localized Excitons in an Atomically Thin Semiconductor. *Optica* **2015**, *2*, 347−352.

(13) Chakraborty, C.; Goodfellow, K. M.; Vamivakas, A. N. Localized Emission from Defects in $MoSe_2$ Layers. *Opt. Mater. Express* **2016**, *6*, 2081−2087.

(14) Tran, T. T.; Bray, K.; Ford, M. J.; Toth, M.; Aharonovich, I. Quantum Emission from Hexagonal Boron Nitride Monolayers. *Nat. Nanotechnol.* **2016**, *11*, 37−41.

(15) Li, X.; Shepard, G. D.; Cupo, A.; Camporeale, N.; Shayan, K.; Luo, Y.; Meunier, V.; Strauf, S. Nonmagnetic Quantum Emitters in Boron Nitride with Ultranarrow and Sideband-Free Emission Spectra. *ACS Nano* **2017**, *11*, 6652−6660.

(16) Tonndorf, P.; Schwarz, S.; Kern, J.; Niehues, I.; Pozo-Zamudio, O. D.; Dmitriev, A. I.; Bakhtinov, A. P.; Borisenko, D. N.; Kolesnikov, N. N.; Tartakovskii, A. I.; Michaelis de Vasconcellos, S.; Bratschitsch, R. Single-Photon Emitters in GaSe. *2D Mater.* **2017**, *4*, 021010.

(17) Kumar, S.; Kaczmarczyk, A.; Gerardot, B. D. Strain-Induced Spatial and Spectral Isolation of Quantum Emitters in Mono- and Bilayer WSe_2. *Nano Lett.* **2015**, *15*, 7567−7573.

(18) Kern, J.; Niehues, I.; Tonndorf, P.; Schmidt, R.; Wigger, D.; Schneider, R.; Stiehm, T.; Michaelis de Vasconcellos, S.; Reiter, D. E.; Kuhn, T.; Bratschitsch, R. Nanoscale Positioning of Single-Photon Emitters in Atomically Thin WSe_2. *Adv. Mater.* **2016**, *28*, 7101−7105.

(19) Shepard, G. D.; Ajayi, O. A.; Li, X.; Zhu, X.-Y.; Hone, J.; Strauf, S. Nanobubble Induced Formation of Quantum Emitters in Monolayer Semiconductors. *2D Mater.* **2017**, *4*, 021019.

(20) Branny, A.; Kumar, S.; Proux, R.; Gerardot, B. D. Deterministic Strain-Induced Arrays of Quantum Emitters in a Two-Dimensional Semiconductor. *Nat. Commun.* **2017**, *8*, 15053.

(21) Palacios-Berraquero, C.; Kara, D. M.; Montblanch, A. R.-P.; Barbone, M.; Latawiec, P.; Yoon, D.; Ott, A. K.; Loncar, M.; Ferrari, A. C.; Atatüre, M. Large-Scale Quantum-Emitter Arrays in Atomically Thin Semiconductors. *Nat. Commun.* **2017**, *8*, 15093.

(22) Cai, T.; Dutta, S.; Aghaeimeibodi, S.; Yang, Z.; Nah, S.; Fourkas, J. T.; Waks, E. Coupling Emission from Single Localized Defects in Two-Dimensional Semiconductor to Surface Plasmon Polaritons. *Nano Lett.* **2017**, *17*, 6564−6568.

(23) Proscia, N. V.; Shotan, Z.; Jayakumar, H.; Reddy, P.; Dollar, M.; Alkauskas, A.; Doherty, M.; Meriles, C. A.; Menon, V. M. Near-Deterministic Activation of Room Temperature Quantum Emitters in Hexagonal Boron Nitride. 2017, arXiv:1712.01352 [Cond-Mat, Physics:physics]. https://arxiv.org/abs/1712.01352.

(24) Henzie, J.; Lee, J.; Lee, M. H.; Hasan, W.; Odom, T. W. Nanofabrication of Plasmonic Structures. *Annu. Rev. Phys. Chem.* **2009**, *60*, 147−165.

(25) Barnes, W. L.; Dereux, A.; Ebbesen, T. W. Surface Plasmon Subwavelength Optics. *Nature* **2003**, *424*, 824−830.

(26) Schuller, J. A.; Barnard, E. S.; Cai, W.; Jun, Y. C.; White, J. S.; Brongersma, M. L. Plasmonics for Extreme Light Concentration and Manipulation. *Nat. Mater.* **2010**, *9*, 193−204.

DOI: 10.1021/acsphotonics.8b00580
ACS Photonics 2018, 5, 3466−3471

(27) Hoang, T. B.; Akselrod, G. M.; Mikkelsen, M. H. Ultrafast Room-Temperature Single Photon Emission from Quantum Dots Coupled to Plasmonic Nanocavities. *Nano Lett.* **2016**, *16*, 270−275.
(28) Hoang, T. B.; Akselrod, G. M.; Argyropoulos, C.; Huang, J.; Smith, D. R.; Mikkelsen, M. H. Ultrafast Spontaneous Emission Source Using Plasmonic Nanoantennas. *Nat. Commun.* **2015**, *6*, 7788.
(29) Waks, E.; Sridharan, D. Cavity QED Treatment of Interactions between a Metal Nanoparticle and a Dipole Emitter. *Phys. Rev. A: At., Mol., Opt. Phys.* **2010**, *82*, 043845.
(30) Vesseur, E. J. R.; de Abajo, F. J. G.; Polman, A. Broadband Purcell Enhancement in Plasmonic Ring Cavities. *Phys. Rev. B: Condens. Matter Mater. Phys.* **2010**, *82*, 165419.
(31) Koenderink, A. F. On the Use of Purcell Factors for Plasmon Antennas. *Opt. Lett.* **2010**, *35*, 4208−4210.
(32) Nguyen, M.; Kim, S.; Tran, T. T.; Xu, Z.-Q.; Kianinia, M.; Toth, M.; Aharonovich, I. Nanoassembly of Quantum Emitters in Hexagonal Boron Nitride and Gold Nanospheres. *Nanoscale* **2018**, *10*, 2267−2274.
(33) Tran, T. T.; Wang, D.; Xu, Z.-Q.; Yang, A.; Toth, M.; Odom, T. W.; Aharonovich, I. Deterministic Coupling of Quantum Emitters in 2D Materials to Plasmonic Nanocavity Arrays. *Nano Lett.* **2017**, *17*, 2634−2639.
(34) Tripathi, L. N.; Iff, O.; Betzold, S.; Emmerling, M.; Moon, K.; Lee, Y. J.; Kwon, S.-H.; Höfling, S.; Schneider, C. Spontaneous Emission Enhancement in Strain-Induced WSe_2 Monolayer Based Quantum Light Sources on Metallic Surfaces. 2017, arXiv:1709.00631 [Cond-Mat]. https://arxiv.org/abs/1709.00631.
(35) Varcoe, B. T. H.; Brattke, S.; Weidinger, M.; Walther, H. Preparing Pure Photon Number States of the Radiation Field. *Nature* **2000**, *403*, 743−746.
(36) Hofheinz, M.; Weig, E. M.; Ansmann, M.; Bialczak, R. C.; Lucero, E.; Neeley, M.; O'Connell, A. D.; Wang, H.; Martinis, J. M.; Cleland, A. N. Generation of Fock States in a Superconducting Quantum Circuit. *Nature* **2008**, *454*, 310−314.
(37) Hofheinz, M.; Wang, H.; Ansmann, M.; Bialczak, R. C.; Lucero, E.; Neeley, M.; O'Connell, A. D.; Sank, D.; Wenner, J.; Martinis, J. M.; Cleland, A. N. Synthesizing Arbitrary Quantum States in a Superconducting Resonator. *Nature* **2009**, *459*, 546−549.
(38) Bose, R.; Cai, T.; Choudhury, K. R.; Solomon, G. S.; Waks, E. All-Optical Coherent Control of Vacuum Rabi Oscillations. *Nat. Photonics* **2014**, *8*, 858−864.
(39) Anger, P.; Bharadwaj, P.; Novotny, L. Enhancement and Quenching of Single-Molecule Fluorescence. *Phys. Rev. Lett.* **2006**, *96*, 113002.
(40) Huang, J.-K.; Pu, J.; Hsu, C.-L.; Chiu, M.-H.; Juang, Z.-Y.; Chang, Y.-H.; Chang, W.-H.; Iwasa, Y.; Takenobu, T.; Li, L.-J. Large-Area Synthesis of Highly Crystalline WSe_2 Monolayers and Device Applications. *ACS Nano* **2014**, *8*, 923−930.
(41) Castellanos-Gomez, A.; Buscema, M.; Molenaar, R.; Singh, V.; Janssen, L.; van der Zant, H. S. J.; Steele, G. A. Deterministic Transfer of Two-Dimensional Materials by All-Dry Viscoelastic Stamping. *2D Mater.* **2014**, *1*, 011002.
(42) He, Y.-M.; Hofling, S.; Schneider, C. Phonon induced line broadening and population of the dark exciton in a deeply trapped localized emitter in monolayer WSe_2. *Opt. Express* **2016**, *24*, 8066−8073.
(43) Exarhos, A. L.; Hopper, D. A.; Grote, R. R.; Alkauskas, A.; Bassett, L. C. Optical Signatures of Quantum Emitters in Suspended Hexagonal Boron Nitride. *ACS Nano* **2017**, *11*, 3328−3336.
(44) He, Y.-M.; Iff, O.; Lundt, N.; Baumann, V.; Davanco, M.; Srinivasan, K.; Höfling, S.; Schneider, C. Cascaded emission of single photons from the biexciton in monolayered WSe_2. *Nat. Commun.* **2016**, *7*, 13409.
(45) Grosso, G.; Moon, H.; Lienhard, B.; Ali, S.; Efetov, D. K.; Furchi, M. M.; Jarillo-Herrero, P.; Ford, M. J.; Aharonovich, I.; Englund, D. Tunable and high-purity room temperature single-photon emission from atomic defects in hexagonal boron nitride. *Nat. Commun.* **2017**, *8*, 705.

DOI: 10.1021/acsphotonics.8b00580
ACS Photonics 2018, 5, 3466−3471